J. Fluid Mech. (1986), *vol.* 164, *pp.* 1–25
Printed in Great Britain

Wake interference of a row of normal flat plates arranged side by side in a uniform flow

By MASANORI HAYASHI, AKIRA SAKURAI
Department of Aeronautical Engineering, Faculty of Engineering, Kyushu University, Fukuoka, 812, Japan

AND YUJI OHYA
Department of Resource Development and Mechanical Engineering, Faculty of Engineering, Kumamoto University, Kumamoto, 860, Japan

(Received 17 January 1985 and in revised form 25 September 1985)

The wake characteristic of groups of normal flat plates, consisting of two, three, or four plates placed side by side with slits in between, have been investigated experimentally. When the ratio of the slit width to the plate width (slit ratio) was small, the gap flows were observed to be biased either upward or downward in a stable way, leading to multiple, stable flow patterns for a single slit-ratio value. Some regularities were recognized in the gap-flow directions and the appearance of the flow patterns. The plates on the biased side showed high drag and regular vortex shedding, while those on the unbiased side showed the opposite. The origin of the biased flow has also been investigated with water-tank experiments, numerical calculations and wind-tunnel experiments. The results showed that the origin of biasing is strongly related to the vortex shedding of each plate of a row.

1. Introduction

When more than one bluff body is placed in a uniform flow, the aerodynamic parameters and vortex-shedding patterns are completely different from the case of a single body, because their wakes or vortex streets interfere in a complex manner, depending on the arrangement or spacing of the plates.

Although this has been known for a long time, recent engineering problems such as the local strong wind around a group of skyscrapers, and the flow-induced vibration of tubes in heat exchangers, bridges, or marine structures have necessitated detailed investigations of flow patterns and aerodynamic characteristics about multiple bluff bodies. It is also an interesting example of nonlinear interaction problems in fluid dynamics.

Many experimental investigations have been carried out, especially on flows around groups of circular cylinders. These include Biermann & Herrnstein (1933), Spivack (1946), Hori (1959), Ishigai *et al.* (1972), Bearman & Wadcock (1973), Honji (1973*a*, *b*), Zdravkovich (1977), Quadflieg (1977) and Okajima & Sugitani (1980). It is known, for example, that, when two circular cylinders are placed side by side in the approaching flow and the gap between them is small, the flow passing through the gap becomes biased to one side, and the two cylinders show different wakes, drags, lifts and vortex-shedding frequencies. Kamemoto (1976), Kamemoto & Bearman (1980) and Stansby (1981) carried out theoretical analyses of the wakes of two bluff bodies placed side by side, by modelling the flow with vortex sheets or point-vortex

rows. However, most of the aerodynamic interference phenomena around multiple bluff bodies and their origins still remain to be clarified.

In the present experiment, normal flat plates were selected as typical of bluff bodies, and the wake interference behind a row of two, three, or four plates placed side by side in a uniform flow was investigated.

The most striking feature observed in the flow behind multiple bluff bodies in the side-by-side arrangement is that the gap flow is biased to one side in a stable or unstable manner. Bearman & Wadcock (1973) suggested that the biasing of gap flow is due to a near-wake phenomenon rather than being related to the position of boundary-layer separation. Zdravkovich (1977) made a similar suggestion and stated that the bistable side-by-side arrangement for a pair of circular cylinders represents a transition between the two staggered arrangements, i.e. from the upstream to the downstream stagger (or *vice versa*). On the other hand, Quadflieg (1977) insisted that the gap flow becomes a jet-like flow, so the Coanda effect causes the biasing.

Since the origin of the biasing is not yet clear, it is interesting to see if it also occurs in laminar, low-Reynolds-number flows. If so, the turbulence which is characteristic of the high-Reynolds-number wakes may be omitted from the principal causes of the biasing phenomenon. One of the objects of the present paper is, therefore, to investigate the wake interference of two normal flat plates arranged side by side to a uniform flow at low Reynolds numbers (below 100) with water-tank experiments and numerical calculations and to determine if the wake biasing occurs.

The other object of this study is to give some physical insight into the origin of the biased gap flow by noting the vortex shedding of each plate of a row. When the vortex shedding of each plate of a flat-plate row is impeded by an artificial disturbance, like a guide vane or small fins attached to the plates of a row, it is also interesting to examine what kind of wake interference appears behind the flat-plate row.

2. Wind-tunnel experiments

2.1. *Experimental methods*

A row of normal flat plates was placed in a wind tunnel of open section diameter 2 m. Each row consisted of two, three, or four normal flat plates placed side by side with equal slit width s as shown in figure 1. In most cases, the slit ratio, s/d, was altered by changing s while keeping the width of individual plate d constant at 30 mm. In the case of four-plate rows with s/d less than 1.5, however, s/d was altered by changing d while keeping the overall height h constant at 80 mm. Porosity β (the ratio of the sum of gaps s to the overall height h of a row) is defined as another parameter. Each plate was 700 mm long. The aspect ratios of flat plates ranged from 8.8 to 74. Glass end-plates 910×1490 mm were placed at the model ends to ensure an approximately two-dimensional flow field. Most experiments were carried out at free-stream velocity U_0 of 7–11 m/s, with corresponding Reynolds numbers of $Re = (0.6\text{–}1.9) \times 10^4$ in terms of d.

The surface static pressure was measured using pressure taps of 0.3 mm diameter. The pressure was determined with a multitube alcohol manometer, and the mean pressure p was presented in the form of a pressure coefficient $C_p = (p-p_0)/(\frac{1}{2}\rho U_0^2)$, where ρ and p_0 are respectively the air density and the mean static pressure of the free stream. The drag coefficient C_D was obtained by integrating the pressure distribution. The velocity fluctuation was measured by a hot-wire anemometer. The Strouhal number, defined as $St = fd/U_0$, was estimated from the frequency of the

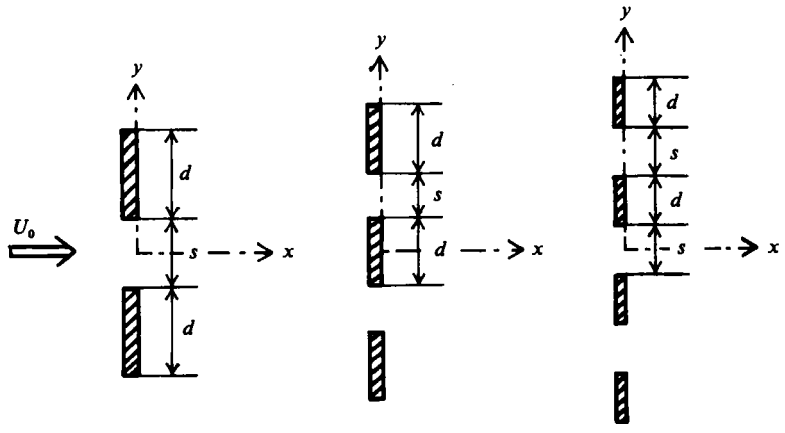

FIGURE 1. Rows of normal flat plates.

u-component velocity fluctuation f. In the case of four-plate rows, a tandem hot-wire probe (Mizota 1978) that can measure the time-mean x-component velocity even in the reversed-flow region was utilized. The flow field was visualized using the smoke-wire technique at a free-stream velocity of around 5 m/s, with Re approximately 10^4.

2.2. *Flow patterns around flat-plate rows*

When a row of multiple flat plates is placed normal to a free stream, the flows passing through the slits (called gap flows henceforth) are biased either upward or downward in a stable manner when the slit ratio s/d is small. Once a biased gap-flow pattern appears, the direction of the biasing remains the same unless some forced disturbance is given. This phenomenon is apparently different from the case of a pair of circular cylinders, where the biased gap flow is not stable but changes direction abruptly at irregular intervals (flip-flapping). In the case of normal flat plates, however, it is only possible to change the direction of biasing by some definite perturbations, for example by inserting a cylinder in front of or behind the row of plates for a moment. Following the change, the new biased flow pattern is again stable. Thus, stable multiple flow patterns are observed at a single s/d value.

2.2.1. *Classification of flow patterns*

The observed flow patterns are shown schematically in figure 2, taken from instantaneous and time-mean flow photographs (Ohya 1983). For future convenience, those in which all the gap flows are biased in the same direction are called pattern A, those in which not all are biased in the same direction, pattern B, and those in which no biasing is observed, pattern C, as shown. The mirror-image patterns occur with the same probability when they exist. The sequence of these flow patterns, which appear with an increasing s/d, is: A only $\rightarrow$ both A and B $\rightarrow$ B only $\rightarrow$ C (A $\rightarrow$ C, for two-plate row). It should be noted that, among different flat-plate rows, the range in which the biased flow exists is almost the same and is about $s/d < 2.0$–2.25. Each plate in a row is given the symbol shown in figure 2.

2.2.2. *Rows of two flat plates*

When s/d is less than 2.0, the gap flow is biased either upward or downward (pattern A). Although this biasing is not stable at $s/d = 1.75$ and a flip-flapping appears, it becomes stable at smaller s/d.

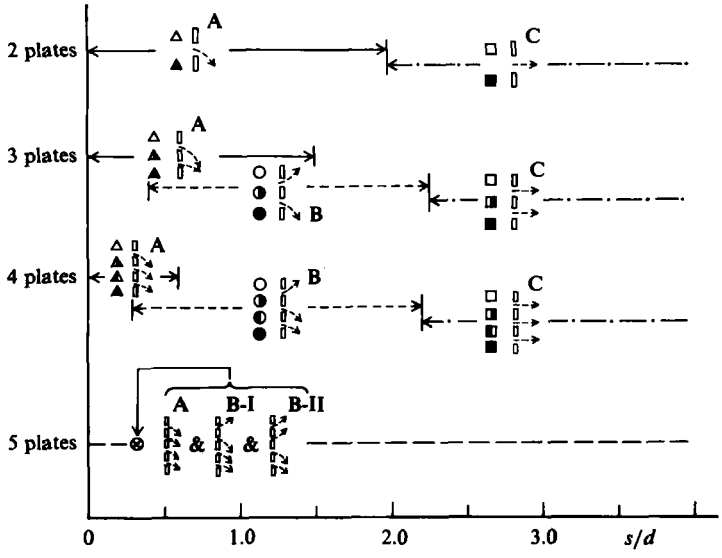

FIGURE 2. Flow patterns around flat-plate rows. Arrows with broken lines show the directions of the gap flows.

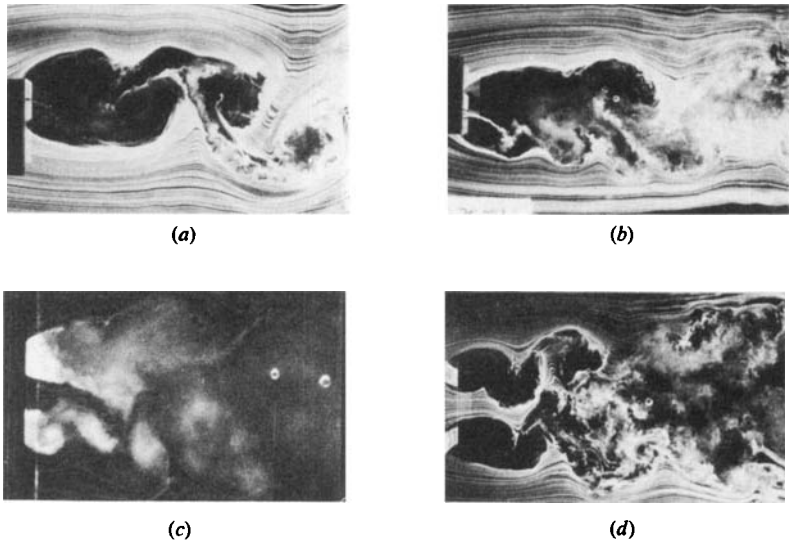

FIGURE 3. Flow visualization behind two-plate rows (instantaneous flow). (*a*) $s/d = 0.2$, pattern A; (*b*) $s/d = 0.75$, pattern A; (*c*) $s/d = 1.5$, pattern A; (*d*) $s/d = 2.5$, pattern C.

When s/d is very small, for example 0.2, the gap flow is weak. Although the vortex shedding by an individual plate is not distinct, the separated shear layers on the outside of both plates interact with each other and roll up to form a large-scale vortex as seen in figure 3(*a*). Three- or four-plate rows with very small slit ratios also show the same phenomenon. Thus the wake behaves like one behind a single flat plate.

Figure 3(*b*) shows an instantaneous flow photograph at $s/d = 0.75$. Thus, when s/d becomes larger than 0.5, the vortex shedding from the plate on the biased side

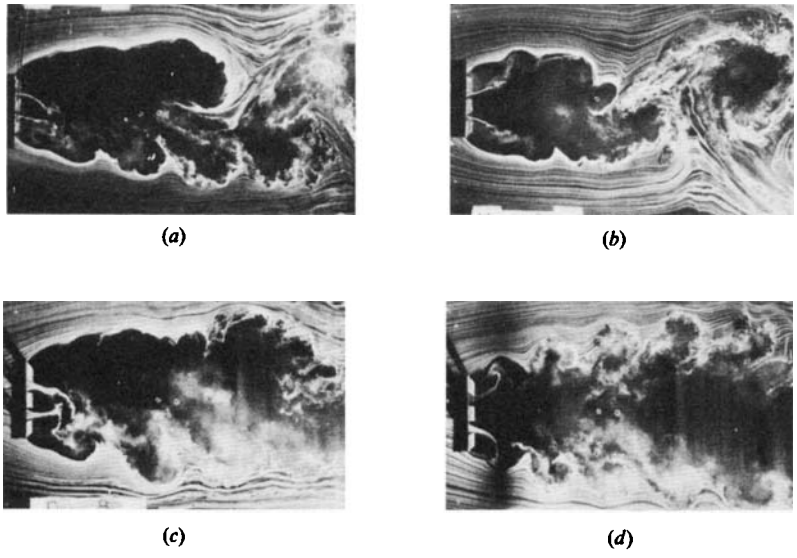

FIGURE 4. Flow visualization behind three-plate rows (instantaneous flow). (*a*) $s/d = 0.5$, pattern A; (*b*) $s/d = 0.5$, pattern B; (*c*) $s/d = 1.0$, pattern A; (*d*) $s/d = 1.0$, pattern B.

becomes distinct, and a small vortex street is formed behind it. No vortex street is observed behind the other plate. The small vortex street on the biased side soon becomes indistinct and is engulfed by a large-scale vortex street formed by the two plates together further downstream.

Up to some value of s/d, a large-scale Kármán vortex street is formed by all plates together at some distance behind the plate row. This phenomenon is similar to that for bluff bodies with base-bleed, which causes the vortex street to be formed further downstream or to disappear (Wood 1964; Bearman 1967; Castro 1971).

When s/d is between 1.25 and 1.75, the shear layers separated from the plate on the biased side roll up sharply behind the plate, as in figure 3(*c*). On the other hand, the separated shear layer from the slit side of the plate on the unbiased side, though strongly influenced by the active vortex formation and shedding on the biased side, begins to roll up. This incipient vortex-street formation on the unbiased side becomes more distinct at $s/d = 1.75$, and is considered to be the cause of the flip-flapping phenomenon observed in this case.

When s/d exceeds 2.0, the flow through the slit no longer shows biasing (pattern C), and the two plates form their own vortex streets equally as in figure 3(*d*). These vortex streets, however, soon deteriorate since the spacing between them is not wide enough for them to develop independently.

2.2.3. *Rows of three flat plates*

In pattern A, as s/d increases to the range $1.0 \leqslant s/d \leqslant 1.5$, the vortex formation of the middle plate as well as the plate on the biassed side becomes distinct, as in figure 4(*c*), where the two gap flows take part in the vortex formation of the middle plate and are subsequently biassed together either upward or downward.

In addition to pattern A, pattern B also appears in the range of $s/d \geqslant 0.4$ as shown in figures 4(*b*, *d*). In this pattern, gap flows are biassed upward and downward in different directions and both outer plates shed distinct vortices. When s/d exceeds

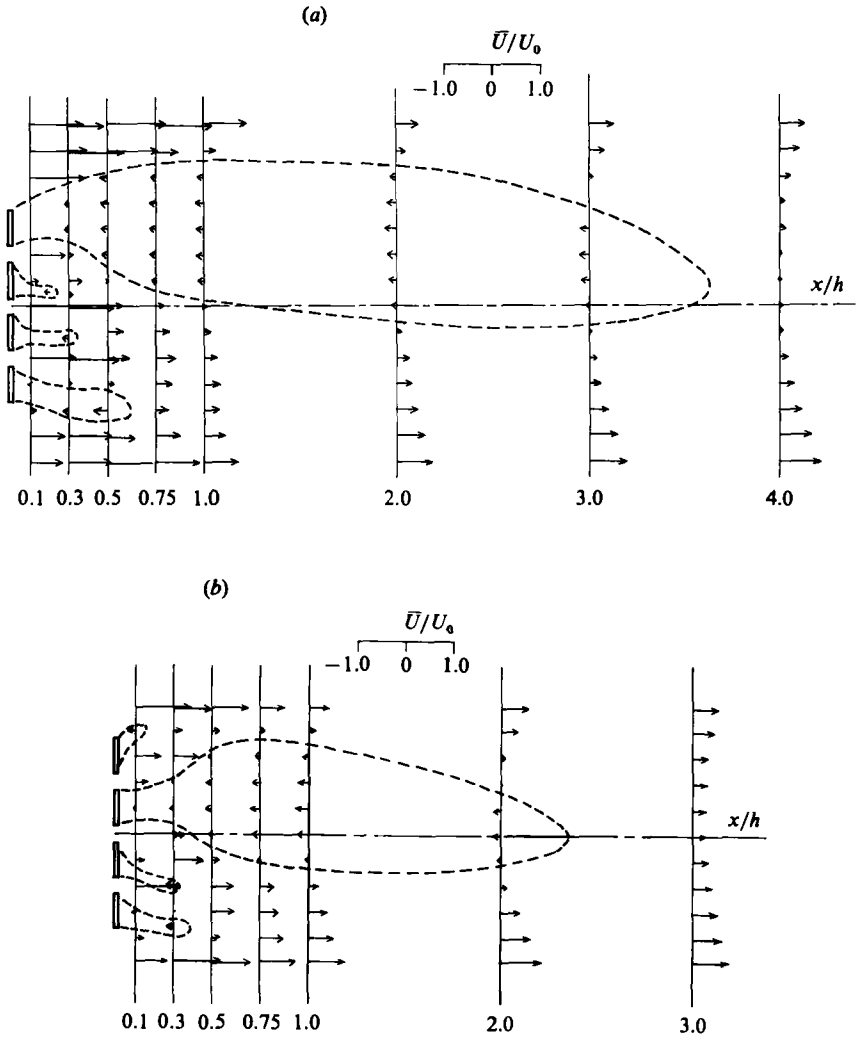

FIGURE 5. Time-mean velocity distribution behind a four-plate row ($s/d = 0.39$ ($\beta = 0.225$)). (*a*) pattern A; (*b*) pattern B.

0.75, the vortex shedding from the two outer plates in pattern B is symmetric with respect to the x-axis, as in figure 4 (*d*).

2.2.4. *Rows of four flat plates*

Figures 5 (*a*, *b*) show the time-mean velocity distribution of both patterns A and B at $s/d = 0.39$ ($\beta = 0.225$). In both patterns, a large reversed-flow region is formed behind the plate on the unbiassed side. Figures 5 (*a*, *b*) correspond to the time-mean flow photographs, figures 6 (*a*, *b*). The position at which the large-scale vortex is formed by the four plates as a whole in pattern B is closer to the plates than in pattern A. This is seen in the difference in the length of the reversed-flow region, which is plotted against s/d in figure 7. The length in pattern B is always shorter than in pattern A.

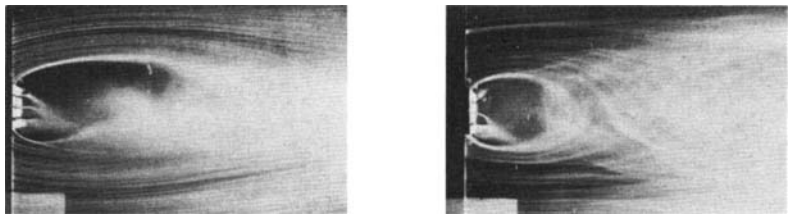

(*a*) (*b*)

FIGURE 6. Flow visualization behind four-plate rows (time-mean flow, $s/d = 0.39$). (*a*) pattern A; (*b*) pattern B.

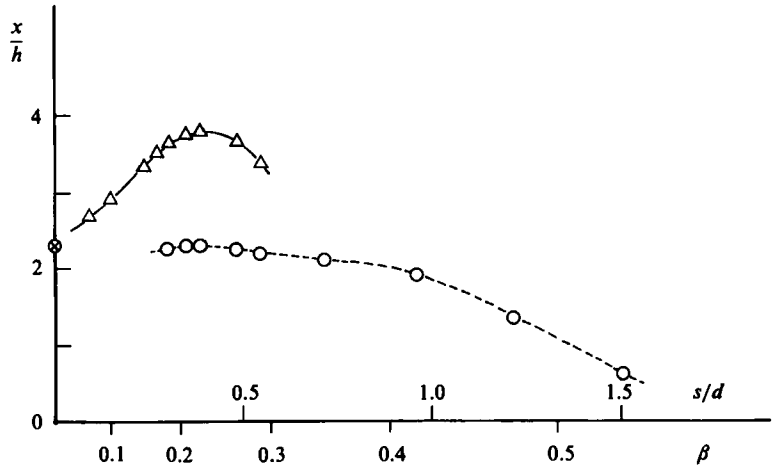

FIGURE 7. The length of reversed-flow region behind four-plate rows. △, pattern A; ○, pattern B; ⊗, single flat plate.

2.2.5. *Some rules of thumb on the existence of flow patterns*

All observed flow patterns are shown schematically in figure 2, which suggests the existence of some rules of thumb on the appearance of flow patterns behind flat-plate rows.

(i) Either all of the gap flows are biassed or none are.

(ii) When the gap flow through one slit is biassed upward (downward), all the gap flows above (below) it are biassed upward (downward). This corresponds to the fact that a large developed back-flow region is attached to the back of only one plate in a row (e.g. figure 5).

(iii) As s/d increases, the gap flows which are biassed in different directions increase.

2.3. *Aerodynamic characteristics of flat-plate rows*

2.3.1. *Drag and base pressure coefficients*

The drag coefficient C_D and the base-pressure coefficient C_{pb} of the individual plates in flat-plate rows are plotted against s/d in figure 8. Figures 8(*a*, *b*) show the contribution of C_{pb} to the variation in C_D. In the two-plate rows of figure 8(*a*), the C_{pb} (or C_D) value at $s/d = 1.75$ changes from one steady value to another (plotted as △ and ▲ in the figure) as the direction of the biassed gap flow changes. The

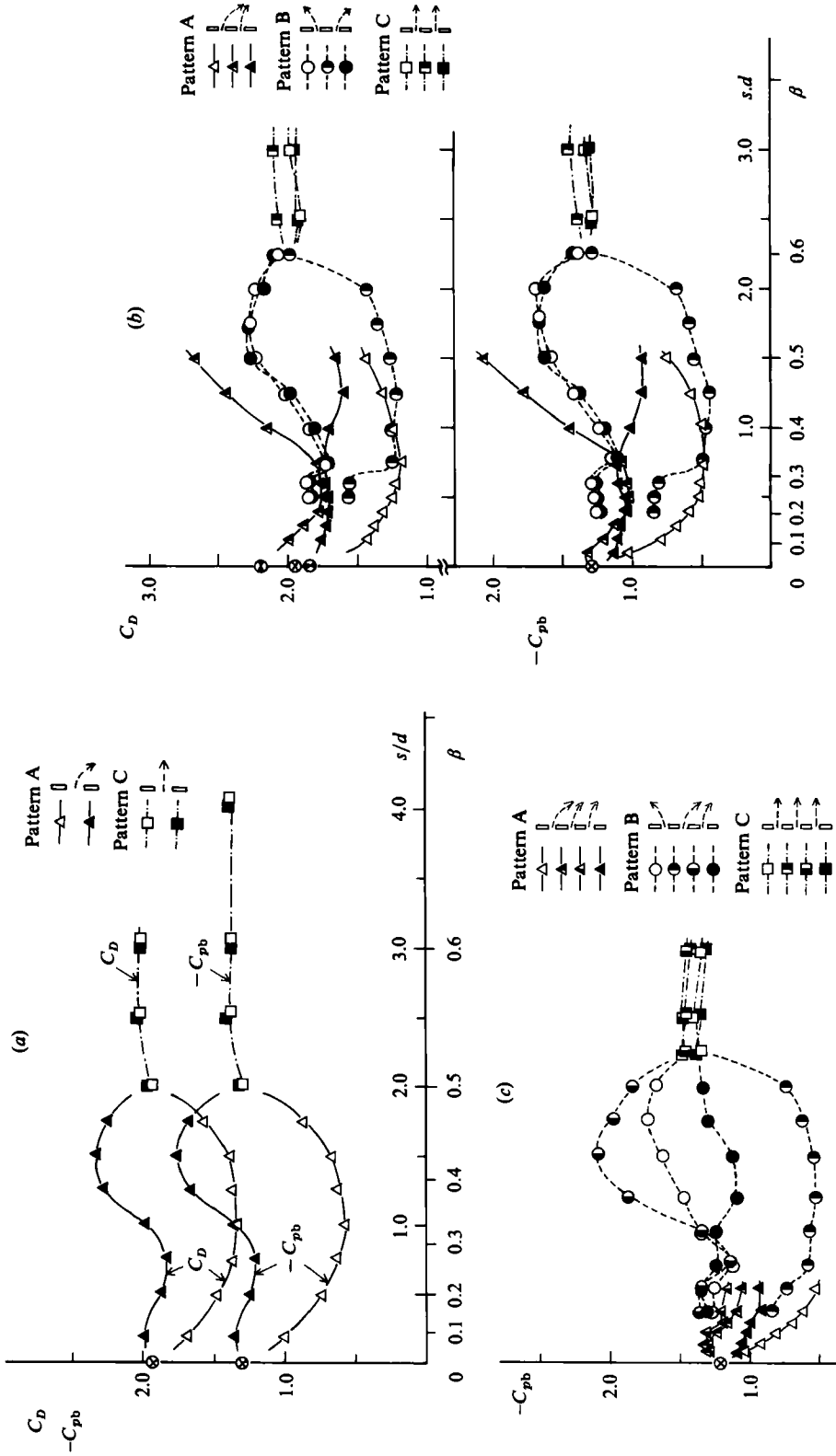

FIGURE 8. Drag and base-pressure coefficients *vs* s/d. ⊗ indicates the case of a single flat plate, i.e. $C_{D\infty}$ and $C_{pb\infty}$. (*a*) Two-plate rows. (*b*) Three-plate rows. ❶ and ❷ are the asymptotic values of C_{pb} for the middle plate and the outer plates respectively, at $s/d \to 0$. (*c*) Four-plate rows.

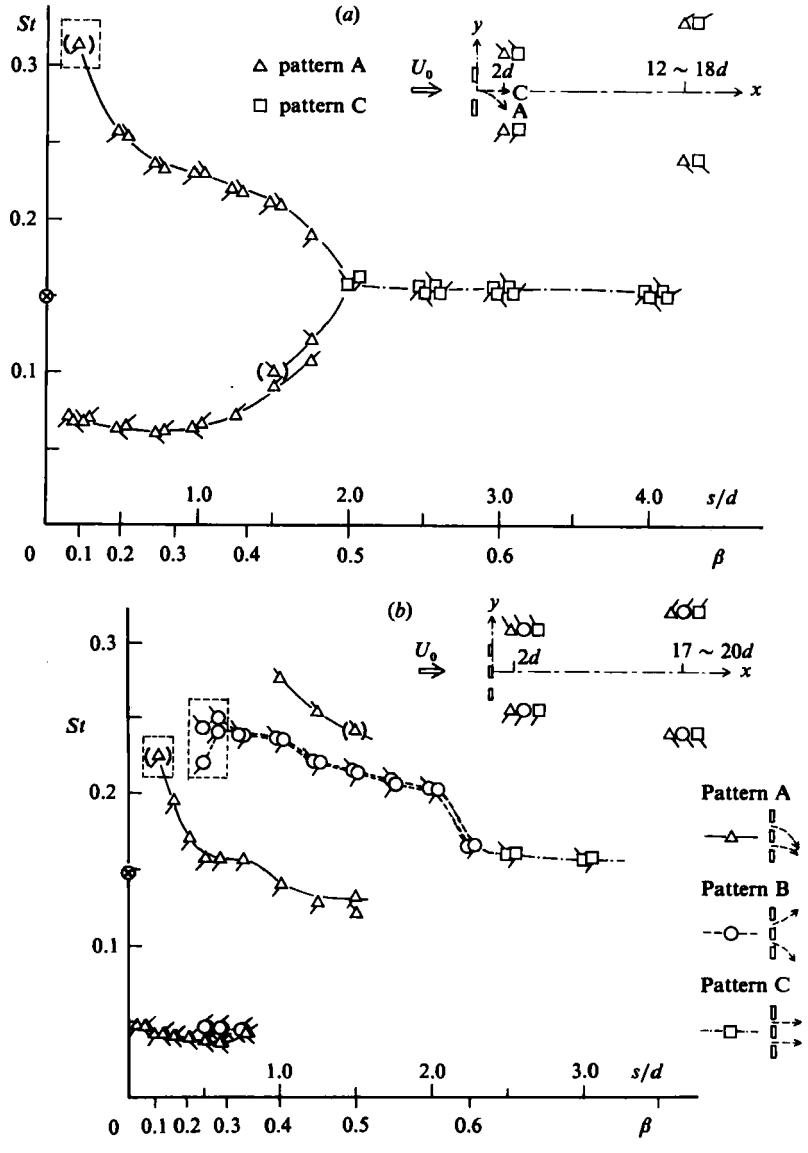

FIGURE 9. Strouhal number *vs* s/d. ⊗, a single flat plate; ( ) and ⬚ correspond respectively to the second peak frequency and a broad peak in the power spectrum. (*a*) Two-plate rows. (*b*) Three-plate rows.

variation of C_{pb} for the two-plate row (figure 8*a*) shows good agreement with Andrepoulos' result cited by Bearman & Wadcock (1973).

With all flat-plate rows in any pattern, the plate to the biassed side of the gap flow shows a lower base pressure. This corresponds to the fact that the plate on the biassed side forms and sheds distinct vortices, except for very small slit ratios, as seen in the photographs in figures 3, 4 and 6.

2.3.2. *Strouhal number*

The Strouhal numbers St for two- and three-plate rows, near ($x = 2d$) and far ($x = 12d$ to $20d$) downstream are plotted against s/d in figures 9(*a*, *b*).

For the two-plate rows in figure 9(*a*), two sets of *St* values are seen in the range of $s/d < 2.0$ where a biassed flow is observed. The higher value is due to a small vortex street from the plate on the biassed side, as seen in figures 3(*b*, *c*). The lower value is due to a large-scale Kármán vortex street formed further downstream when $s/d \leqslant 1.0$, as seen in figures 3(*a*, *b*), and also due to the vortex street which is shed by the plate on the unbiassed side by itself, as seen in figure 3(*c*), when s/d is between 1.25 and 1.75.

For the three-plate rows of figure 9(*b*), *St* varies with the flow pattern. In pattern A, which appears in the range of $s/d \leqslant 1.5$, *St* due to the vortex street of the outer plate on the biassed side as seen in figures 4(*a*, *c*) shows a high value, plotted as ⍋. At $1.0 < s/d < 1.5$ the vortex formation from the middle plate (figure 4*c*) also becomes distinct and *St*, plotted as ⍀, shows a very high value and is almost twice that plotted as ⍋.

In pattern B, the high values of *St*, plotted as ⍥ and ⍴, are due to the vortex shedding of the two outer plates on the biassed side, as seen in figures 4(*b*, *d*). *St* of pattern C in the range of $s/d > 2.25$ is plotted as ⍇ and ⍈ and does not vary with s/d.

The low value of *St* which is seen in the range of $s/d < 1.0$ is due to the large-scale Kármán vortex street formed downstream, as shown in figures 4(*a*, *b*).

2.3.3. *Discussion of aerodynamic characteristics*

From figures 8(*a*–*c*), it can be seen that the overall variation of C_{pb} or C_D with s/d is very similar for two-, three- and four-plate rows. This variation can be roughly divided into three parts, as shown in figure 10. First, when $0 < s/d < 0.75$, the value of C_{pb} increases gradually as s/d becomes larger. Next, when $0.75 < s/d < 2.0$–2.25, the difference in the C_{pb} value for individual plates in the row becomes very large. Finally, when $s/d > 2.0$–2.25, biassed flows are not observed and the C_{pb} value becomes almost constant. Thus, at high slit ratios, the aerodynamic characteristic of each plate in a row becomes close to that of a single flat plate, as shown in figures 8 and 9.

Moreover, the tendencies of C_{pb} in each part are divided into some groups as shown by the circled numbers in figure 10. The individual plate belonging to each group shows a very similar variation of C_{pb}.

As with C_{pb}, the variation in Strouhal number is also found to be independent of the number of plates in the row. For example, the variation (and also the value) of *St* of the plate on the biassed side in two-plate rows (figure 9*a*, plotted as △) agrees with that of the outer plates in pattern B for three-plate rows (figure 9*b*, plotted as ⍥ and ⍴).

As shown schematically in figure 10, it is evident that there are common features between flow fields around the plates belonging to the same group of C_{pb} or *St* variations. In particular, the adjacent gap flows are biassed in the same direction within any group.

According to Biermann & Herrnstein (1933), the total interference drag coefficient of each flat-plate row is defined as

$$C_{D_i} = \frac{\sum_{j=1}^{m} C_{D_j} - mC_{D_\infty}}{m}; \quad m = 2, 3,$$

where C_{D_j} is the drag coefficient of the individual plate and C_{D_∞} is that for a single plate. Figure 11 shows the variation of C_{D_i} with s/d. In the range of s/d where biassed flows are observed, C_{D_i} is most negative, showing that the total drag of the flat-plate

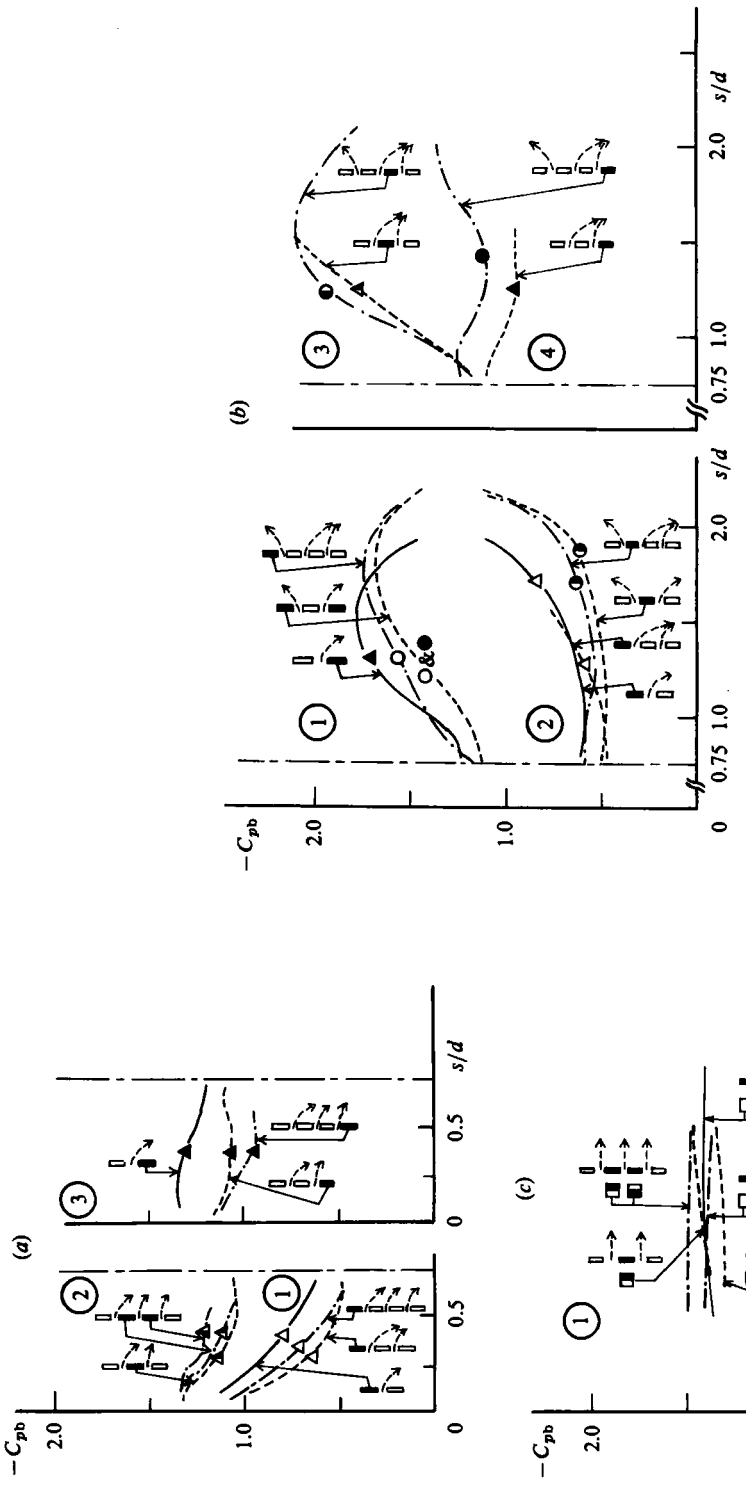

FIGURE 10. Similarities in the C_{pb} variation between flat-plate rows. ——, two-plate rows; – – –, three-plate rows; —·—, four-plate rows. (*a*) $0 < s/d < 0.75$, pattern A; (*b*) $0.75 < s/d < 2.0$–2.25, patterns A and B; (*c*) $s/d > 2.0$–2.25, pattern C.

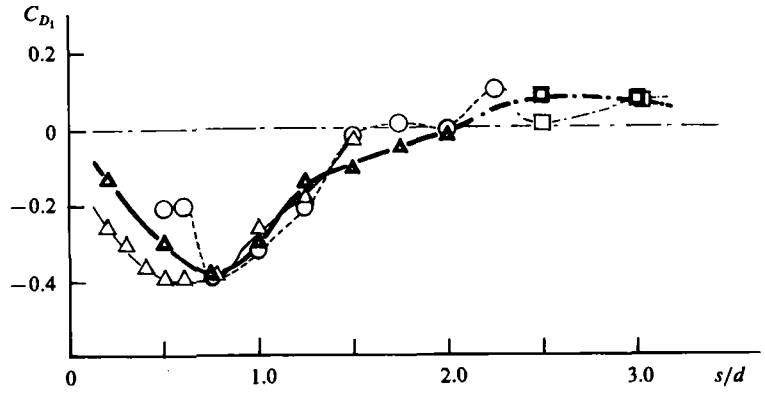

FIGURE 11. Total interference drag coefficient C_{D_1} *vs* s/d. Two-plate rows: ▲, pattern A; ■, pattern C. Three-plate rows: △, pattern A; ○, pattern B, □, pattern C.

row as a whole becomes small because of mutual interference. This suggests that the gap flows play the role of a base-bleed (Wood 1964; Bearman 1967) which is often used as a method of drag reduction. C_{D_1} has a minimum value when s/d is between 0.5 and 0.75, showing that the slit ratio in this range is most effective for reducing the total drag of the flat-plate row.

2.4. *Wake characteristics of four-plate rows as a whole*

Castro (1971) experimentally investigated the wake formed behind two-dimensional perforated plates mounted normal to the air flow. He identified two basic types of wake flows: one in which regular vortex shedding is dominant for plates of low porosity; and the other in which the wake is fully turbulent for plates with high values of porosity. The transition between these two types occurs suddenly at porosity $\beta = 0.2$, causing a kink in the C_D *vs* β curves and a local reduction in St there.

Figure 12 shows the total drag coefficient $C_{D(h)}$ (based on the overall height h) plotted against porosity $\beta(=3s/h)$, which was measured by a six-component balance. Circular end-plates of 700 mm diameter were used in this case only. Figure 13 shows the Strouhal number $St_{(h)}$ (based on the overall height h) against porosity β in the far-downstream position where x/h and y/h are 5–6 and -1.5 to -2.0 respectively. The velocity fluctuation at this location is not caused by a vortex street shed from individual plates but by a large-scale Kármán vortex street formed further downstream, as seen in figures 3 (a, b) and 4 (a, b). Figures 12 and 13 show that pattern B gives rise to higher $C_{D(h)}$ and $St_{(h)}$ values than pattern A at the same porosity β. Castro (1971) suggests a sudden disappearance of the Kármán vortex street as the cause of the kink in C_D and the singularity in St at $\beta = 0.2$ in his two-dimensional perforated-plate experiments. For four-plate rows, however, a Kármán vortex street is clearly observed up to $\beta = 0.417$ ($s/d = 0.96$).

If the number of plates is increased beyond four, the two-dimensional characteristic of the wake behind the flat-plate row would remain. The number of the biassed flow patterns appearing would increase, as shown schematically in figure 2 for a five-plate row with $s/d = 0.32$ (they are depicted from smoke photographs), and hence the flat-plate row would have a different value of $C_{D(h)}$ or $St_{(h)}$ according to the biased flow patterns appearing.

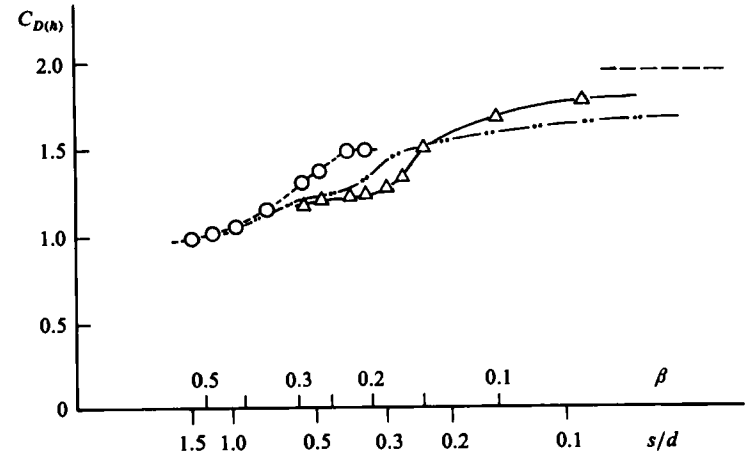

FIGURE 12. Drag coefficient of four-plate rows as a whole (based on the overall height h), $Re_{(h)} = 5.0 \times 10^4$. △, pattern A; ○, pattern B; —··—, Castro (1971), $Re = 9.0 \times 10^4$; ---, a single flat plate.

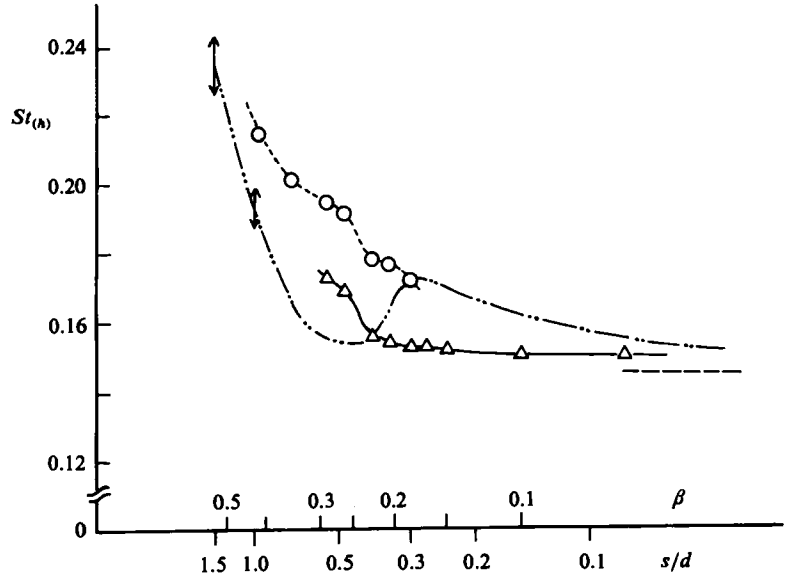

FIGURE 13. Strouhal number of four-plate rows as a whole (based on the overall height h), $Re_{(h)} = 5.0 \times 10^4$. △, pattern A; ○, pattern B; —··—, Castro (1971), $Re = 2.5 \times 10^4$; ---, a single flat plate.

3. Water-tank experiment

3.1. *Experimental apparatus*

The wake interference of two normal flat plates mounted side by side were experimentally investigated in a towing water tank. The tank was 0.45 m wide × 3 m long × 0.62 m deep. Each plate was made of brass 10 mm wide × 2 mm thick × 200 mm long. Four slit ratios, viz. $s/d = 0.5$, 1.0, 1.5 and 2.0, were selected. The flow was visualized using aluminium dust and the electrolytic-precipitation method. The Reynolds number was defined as $Re = Ud/\nu$.

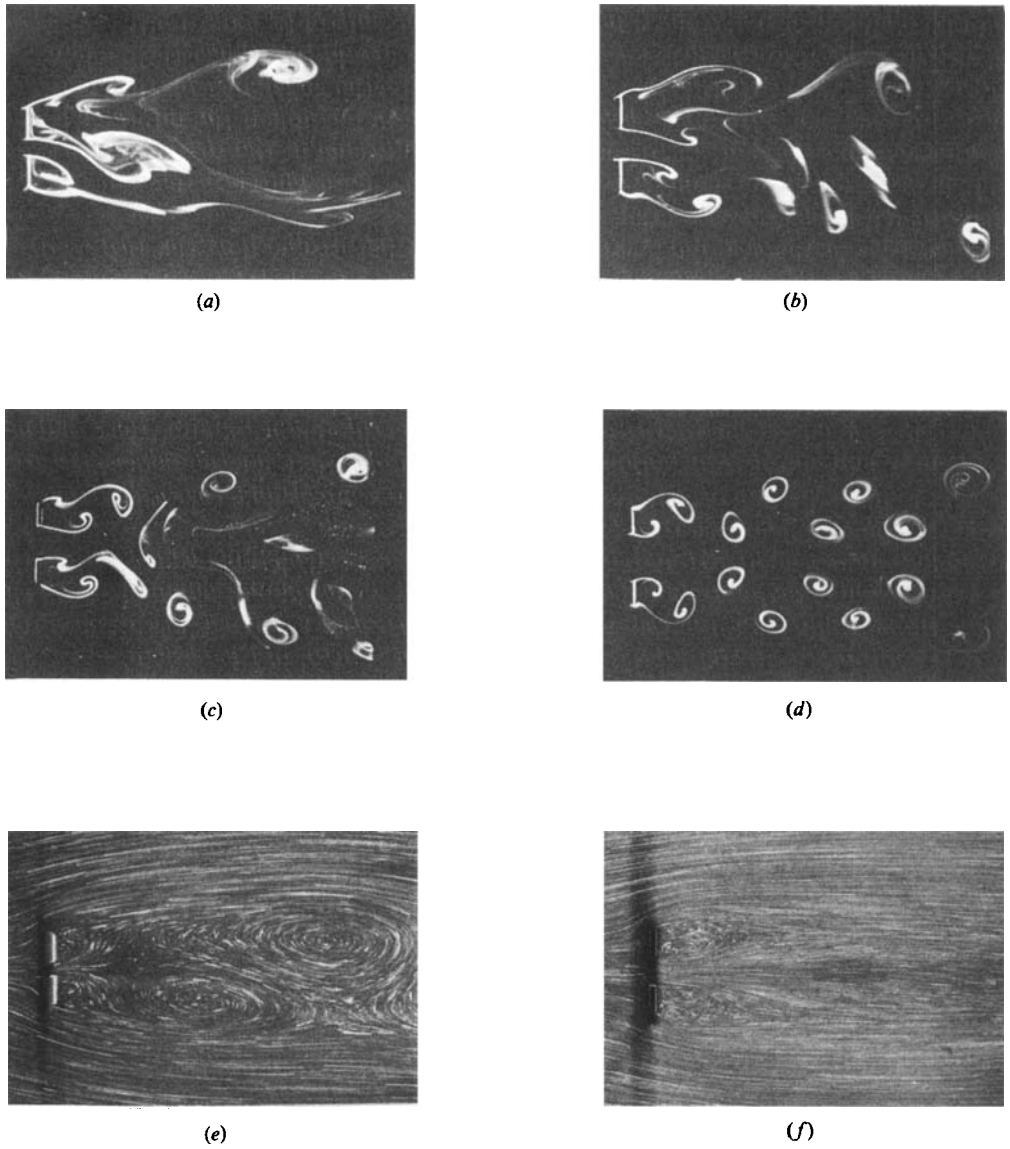

FIGURE 14. Flow visualization behind two-plate rows. (*a*) $s/d = 0.5$, $Re = 59$; (*b*) 1.0, 100; (*c*) 1.5, 100; (*d*) 2.0, 100; (*e*) 0.5, 30; (*f*) 1.0, 30.

3.2. *The wake flow patterns at low Reynolds numbers*

When the slit ratio is small, the gap flow passing through the slit between the plates in a side-by-side arrangement is biassed either upward or downward in a stable way, if the Reynolds number is above 40. Figures 14(*a*, *b*) show the stable, biassed flow patterns with $s/d = 0.5$ at $Re = 59$ and with $s/d = 1.0$ at $Re = 100$, respectively. In these cases, the biassed gap flow is not stable for some time after the model is abruptly started but changes direction at irregular intervals. Then it becomes biassed in one

direction as seen in figures 14(*a*, *b*). The characteristic feature is the wide wake on the unbiassed side and the narrow wake on the biassed side.

With $s/d = 1.5$ and 2.0, the slit is so large that the gap flow is not biassed and the wakes are found to behave independently. With $s/d = 1.5$, vortex shedding is in-phase only for a short initial period and then becomes out-of-phase, as seen in figure 14(*c*). Figure 14(*c*) shows that, in the out-of-phase arrangement, the vortex streets from the inner edges of the plates interact with each other and soon deteriorate. With $s/d = 2.0$, an in-phase vortex arrangement, which is symmetric about the x-axis as seen in figure 14(*d*), is dominant.

Below $Re = 40$, the biassed gap flow does not appear at any slit-ratio value, as shown in figures 14(*e*, *f*). The fact that the biassed gap flow appears at Reynolds numbers above 40 suggests that the origin of the biassed flow is related to the vortex shedding of each plate, because the vortex shedding of a single flat plate also begins at Reynolds number just above 40 (Hayashi 1972).

4. Numerical analysis

The development, after impulsive start, of the flow around two normal flat plates placed between two parallel, stationary walls was considered. Mathematically, an initial-boundary-value problem for the two-dimensional Navier–Stokes equations must be solved. A finite-difference method was used for the numerical calculation (Hayashi, Sakurai & Ohya 1983).

To investigate the biassed flow pattern observed in the flow-visualization experiments in §3, a flow past two flat plates with $s/d = 0.5$ and the depth-to-height ratio of $b/d = 0.2$ was calculated at $Re = 80$, based on d.

To promote the wake interference, an artificial disturbance with upward velocity was superimposed for a short time at the beginning of the calculation in some region behind the plates. As the time increases, first the gap flow becomes biassed in the direction of the artificially introduced disturbance, but then the bias direction changes a few times after the disturbance is removed until it finally settles in one direction. Figure 15 shows the switching of the biassed gap flow from downward to upward. The calculated stream-function lines and the equi-vorticity lines in the figure suggest that the change in the bias direction occurs when two vortices with the same sign of vorticity come close to each other and are finally amalgamated as seen in figures 15(iii–v). Thus the biassed gap flow occurs because of the interaction of vortices shed by the two plates.

Figure 16 shows the variations in C_D and C_L of each plate when the stable biassed flow is being established. Corresponding flow patterns are shown in figures 17(*a*, *b*), which are very similar to those visualized in the water-tank experiments. Figures 16 and 17 show that the two plates experience repulsive lift forces and that the period of C_D and C_L variation differs between the two plates. The wider wake of the lower plate on the unbiassed side is associated with smaller values of mean drag and lift. The smaller vortices shed by the upper plate on the biassed side soon disappear because they are engulfed by the larger vortices from the lower plate. These large vortices develop into a Kármán vortex street formed by the two plates together further downstream.

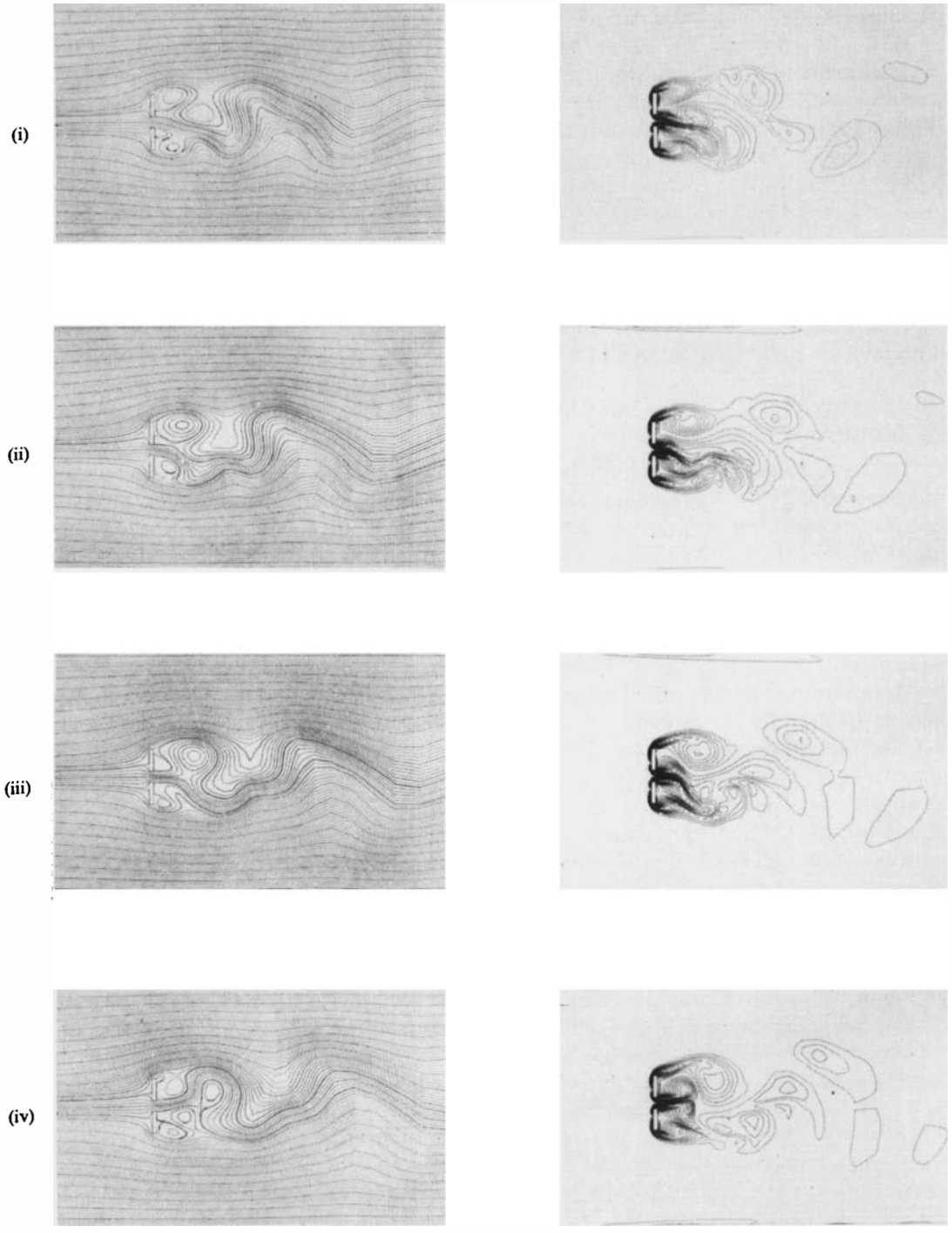

FIGURE 15(i)–(iv). For caption see facing page.

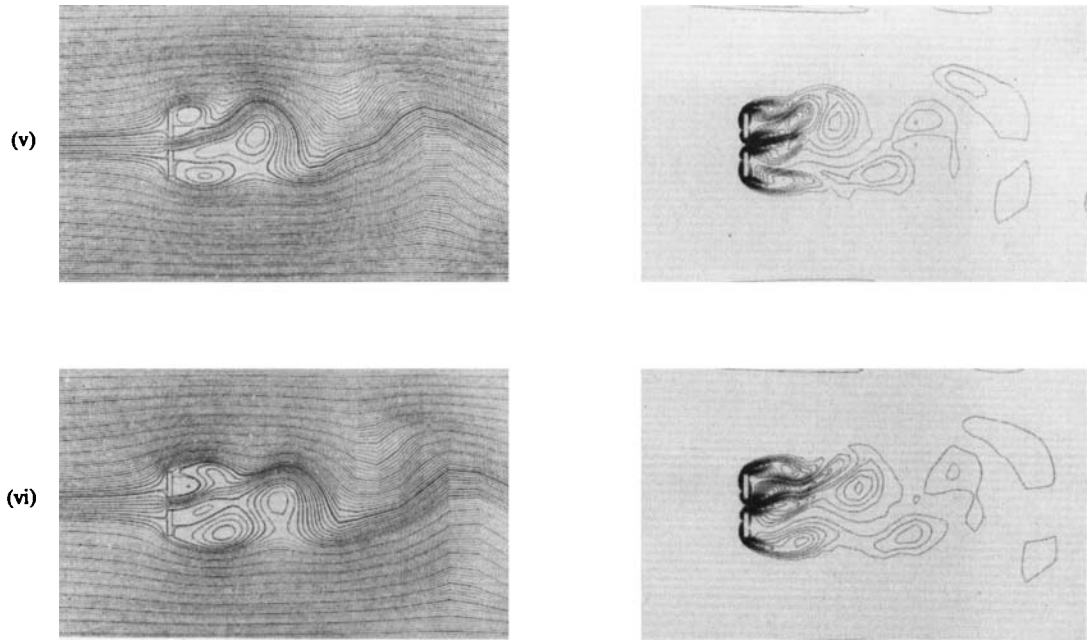

FIGURE 15. Switching of the bias direction of a gap flow: $s/d = 0.5$, $Re = 80$. (*a*) streamlines; (*b*) equi-vorticity lines. (i) $t = 16.5$; (ii) 18.1; (iii) 19.7; (iv) 21.3; (v) 22.9; (vi) 24.5.

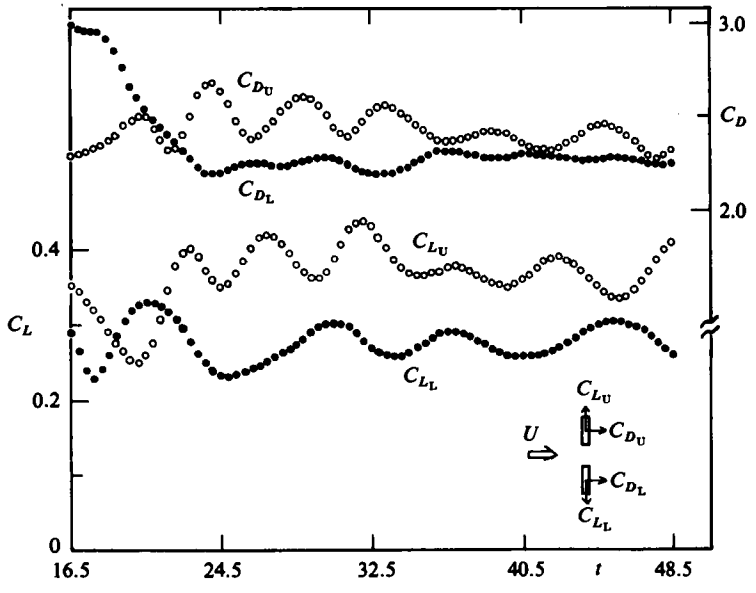

FIGURE 16. Time variations of drag and lift coefficients for two plates with $s/d = 0.5$ at $Re = 80$. The sketch shows the definition of fluid-dynamic forces. C_{D_U} and C_{L_U}, upper plate; C_{D_L} and C_{L_L}, lower plate.

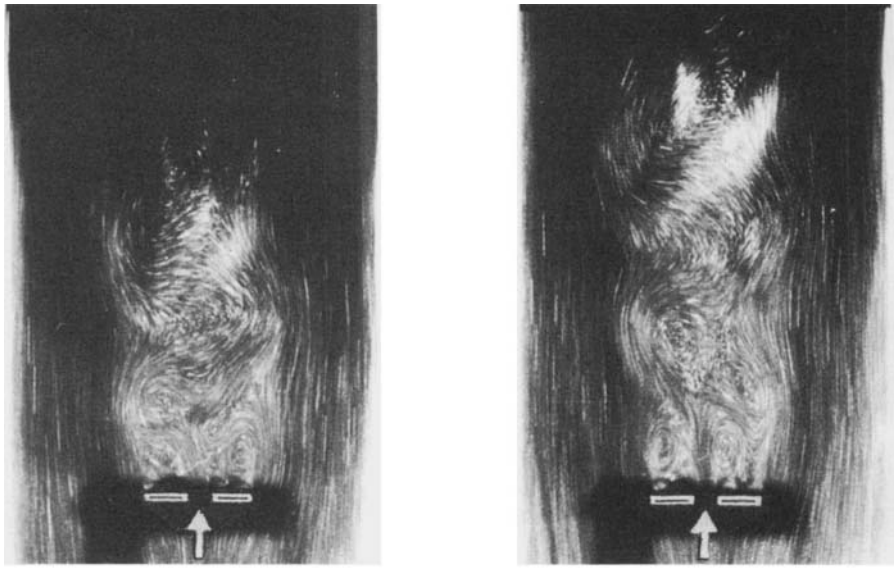

(a)

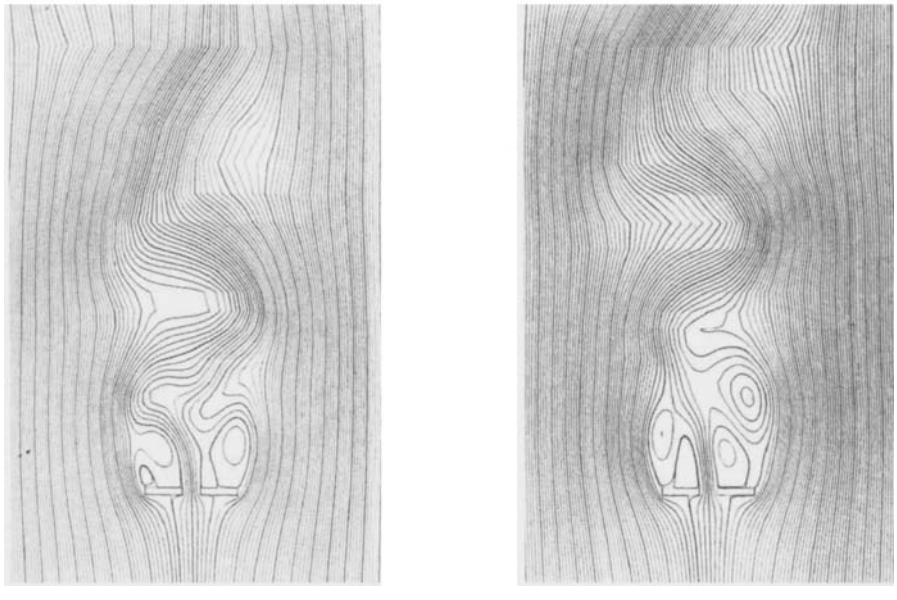

(b) (c)

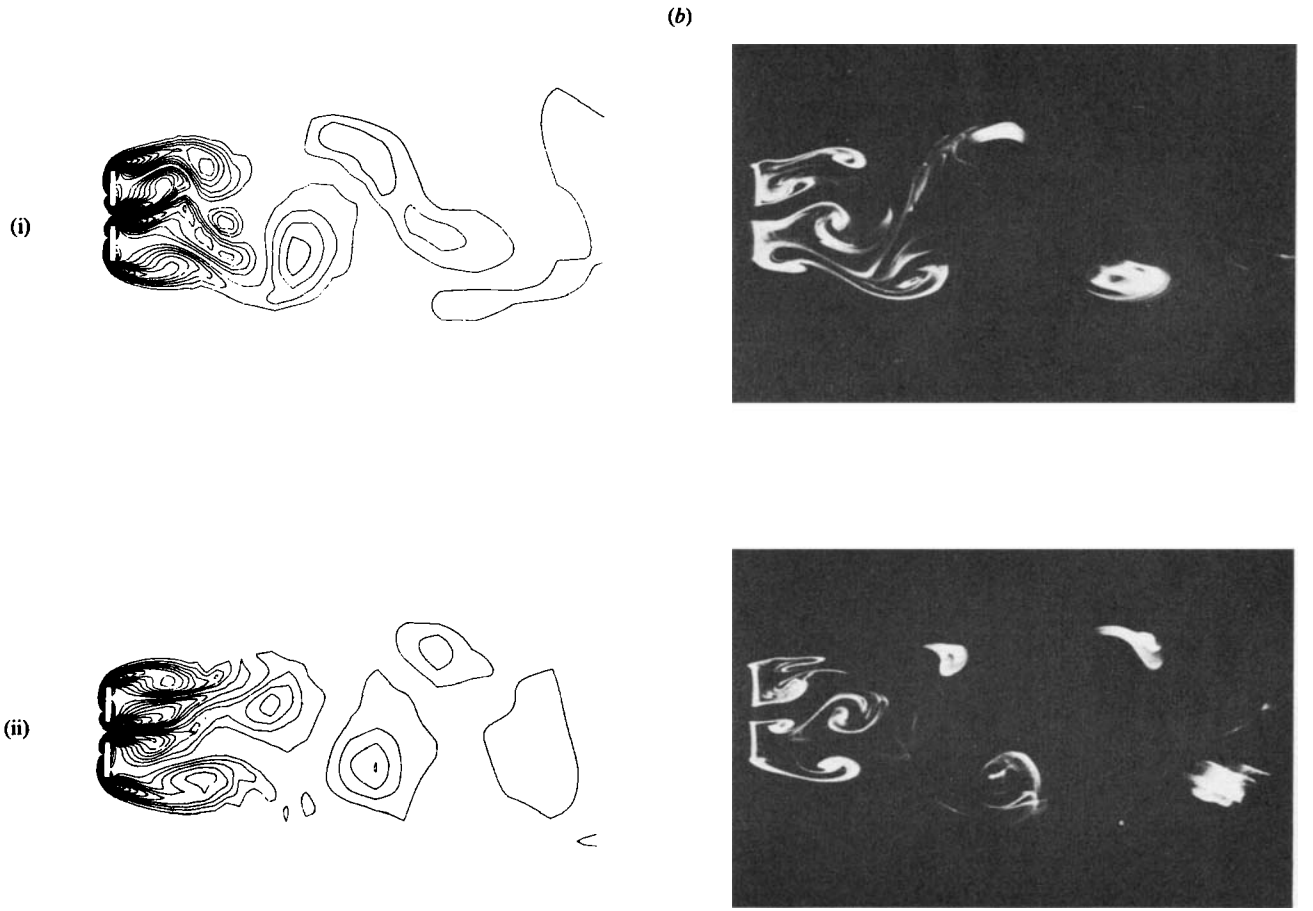

FIGURE 17. Comparison between the calculated and experimental flow patterns around two plates with $s/d = 0.5$ at $Re = 80$. (a) streamlines. (b) equi-vorticity lines. (i) $t = 30.9$; (ii) 34.1.

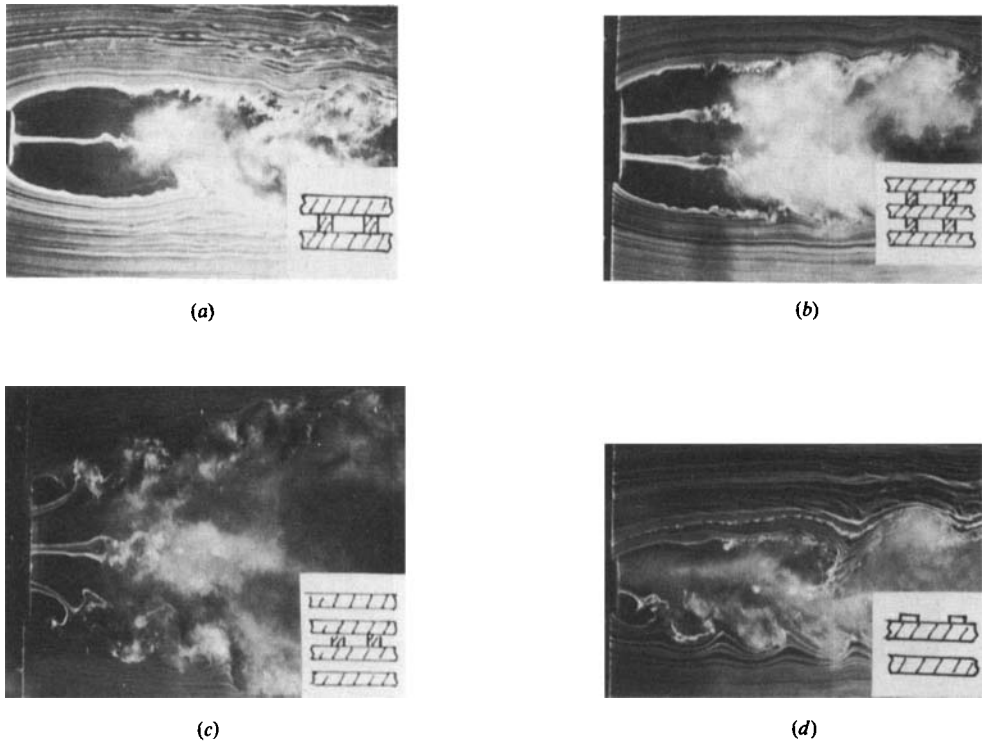

(a) (b)

(c) (d)

FIGURE 18. Flow behind a flat-plate row with small fins. (a) Two-plate row with $s/d = 1.0$; (b) three-plate row with $s/d = 1.0$; (c) four-plate row with $s/d = 1.25$; (d) two-plate row with $s/d = 1.0$.

5. The biassed flow behind a flat-plate row

The water-tank experiments in §3 and numerical investigation in §4 show that the origin of biassed gap flows is strongly related to the vortex shedding of each plate of a flat-plate row. The objective of this section is to investigate the origin of the biassed flow at high Reynolds numbers of about 10^4, by noting the vortex shedding of each plate in the row.

5.1. *Introduction of three-dimensional disturbance*

Vortex shedding of each plate of a flat-plate row was suppressed by small spanwise fins attached to the plates with some separation in between, as depicted in figure 18. When all the plates of a row are prevented from shedding vortices, the gap flows are not biassed, as seen in figure 18(*a*) for a two-plate row with $s/d = 1.0$ and in 18(*b*) for a three-plate row with $s/d = 1.0$. Figure 18(*c*) shows the case of a four-plate row with $s/d = 1.25$ that is prevented from shedding vortices from the inner plates. This flow pattern only appears when there is a disturbance. When the small fins (height $0.33d$) are attached only to the upper plate of a two-plate row with $s/d = 1.0$, the gap flow is always biassed downward, as seen in figure 18(*d*).

5.2. *Attachment of a guide vane*

A guide vane (length $2d$) was attached to the base edge of the upper plate of a two-plate row, as shown in the sketches of figures 19(*a*, *b*). Figure 19(*a*) shows the case of $s/d = 0.2$, where the gap flow is biassed towards the upper plate with the guide vane,

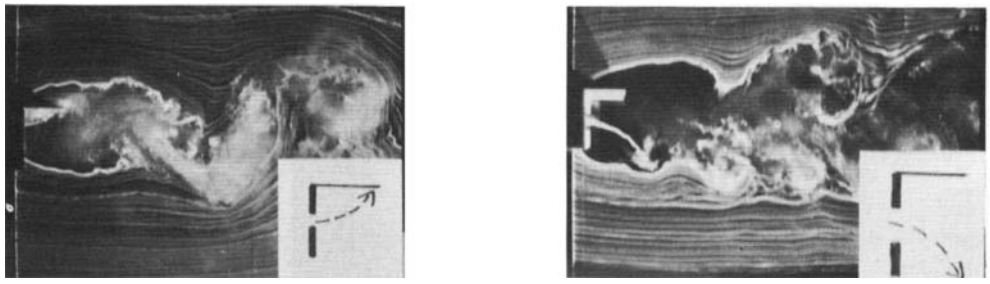

(*a*) (*b*)

FIGURE 19. Flow behind a two-plate row with a guide vane attached to the upper plate. (*a*) $s/d = 0.2$; (*b*) 1.0.

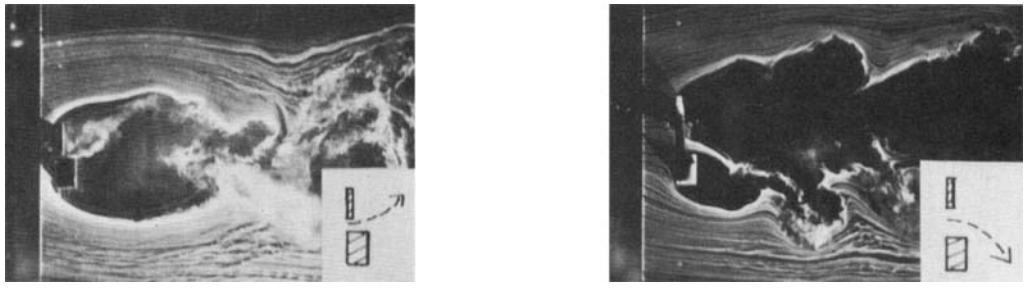

(*a*) (*b*)

FIGURE 20. Flow behind two rectangular cylinders with different depth-to-height ratios, $b/d = 0.2$ (upper) and 1.0 (lower). (*a*) $s/d = 0.2$; (*b*) 1.0.

while, in the case of $s/d = 1.0$, the gap flow is biassed towards the lower plate without the guide vane (figure 19*b*).

5.3. *Different rectangular shape*

It is widely known that the drag forces and the rolling up of the separated shear layers for rectangular cylinders vary with the depth-to-height ratio b/d of the sections (Nakaguchi, Hashimoto & Muto 1968; Bearman & Trueman 1973). Two rectangular cylinders with different depth-to-height ratios were placed side by side, aligning the front faces with respect to the approaching flow. One has $b/d = 0.66$ which shows the strong rolling-up of shear layers and very high drag, while the other has $b/d = 0.2$, which is aerodynamically similar to a normal flat plate. When the slit ratio is very small ($s/d = 0.2$), the gap flow is biassed towards the cylinder with $b/d = 0.2$ (figure 20*a*); on the other hand, when $s/d = 1.0$, the gap flow is biassed towards the cylinder with $b/d = 0.66$ (figure 20*b*).

5.4. *Stability of a biassed gap flow*

The behaviour of the gap flow was also examined using a 16 mm high-speed cine camera in the visualized flow field around a two-plate row with $s/d = 1.0$. Figure 21 is a time sequence of photographs of one cycle of vortex shedding of the lower plate on the biassed side, showing that the separated shear layer from the slit side of the upper plate (unbiassed side) is always engulfed into the vortices shed regularly by

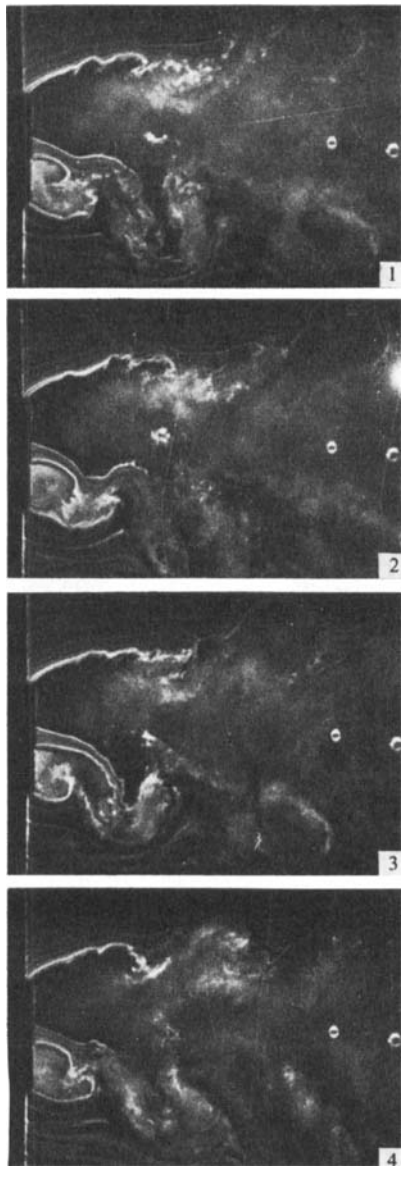

FIGURE 21. Stable biassing of a gap flow for a two-plate row with $s/d = 1.0$.

the lower plate (biassed side). So it is difficult for the upper plate to produce vortices by itself.

Figure 22, on the other hand, shows the case of $s/d = 1.75$, where the gap flow is not stable but changes direction at irregular intervals, similarly to the case of two circular cylinders. It is seen that, although the separated shear layer from the slit side of the upper plate (unbiassed side) is strongly affected by the vortex shedding of the lower plate (biassed side), it can roll up into its own wake and shed distinct vortices. This seems to destabilize the biassing of the gap flow.

FIGURE 22. Unstable biassing of a gap flow for a two-plate row with $s/d = 1.75$.

5.5. *Discussion*

Experiments in suppressing vortex shedding at a high Reynolds number show two different types of wake interference. One is the case of a flat-plate row with a very small slit ratio, where the independent vortex shedding of each plate is weak. The gap flow is biassed towards the plate with a guide vane (figure 19*a*) or towards the rectangular cylinder with $b/d = 0.2$ (figure 20*a*). This suggests that a kind of Coanda effect causes the biassing of the gap flow, since it becomes a jet-like flow through the narrow slit. Here, we assume that a 'Coanda effect' can also be applied to the case of a wall-attaching jet or attaching multiple jets, besides the case of the jet flow attached to a curved surface (Tritton 1977). Therefore, it seems that the biassing of gap flow for very small slit ratios as seen in figure 3(*a*) is caused by a Coanda effect between the jet-like gap flow and the outside flow around the flat-plate row.

The other type of wake interference appears with a flat-plate row with a moderate slit ratio, where each plate of a row is able to shed vortices. The gap flow is biassed towards the plate that sheds vortices more strongly and easily (figures 18*d*, 19*b* and 20*b*). This suggests that the biassing of the gap flow is not caused by a Coanda effect but by the interaction of vortices shed by each plate of a row. That is, the gap flow is engulfed into the stronger vortices and becomes biassed. As seen in figures 18(*a*, *b*), when all the plates of a row are suppressed from vortex shedding, biassing of the gap flow never appears. These results at moderate slit ratios are consistent with the results from water-tank experiments and numerical calculations in low-Reynolds-number flows.

The stability of a biassed flow appears to be particularly dependent on the stability of the separated shear layer from the slit side of the plate on the unbiassed side. A similar suggestion was made by Stansby (1981) in an analysis using a discrete-vortex method for the flow past two circular cylinders side by side.

6. Conclusions

Experimental investigations were made on the wake interference of a row of normal flat plates, consisting of two, three or four plates arranged side by side in a uniform flow with Reynolds numbers of about $(1.3\text{–}1.9) \times 10^4$.

When the slit ratio s/d (the ratio of slit width to plate width), of a row of flat plates is less than about 2.0, the flows through the slits (gap flows) are biassed either upward or downward in a stable way (except for a two-plate row with $s/d = 1.75$ which shows an unstable biassed flow), leading to multiple flow patterns for a single slit-ratio value.

Some regularities were recognized in the wake characteristics of flat-plate rows such as the gap-flow direction and the sequence of appearance of the flow patterns.

The aerodynamic characteristics such as C_D, C_{pb} or St of individual plates vary with the difference in flow patterns. In general, a plate on the biassed side shows higher drag and more regular vortex shedding, while one on the unbiassed side shows the opposite.

Water-tank experiments and numerical calculations at low Reynolds numbers, and wind-tunnel experiments at a high Reynolds number suggested that the origin of the biassed gap flow is related to the interactions of vortices shed by each plate. When the slit ratio is moderate, where each plate of a row can shed vortices, the gap flow is engulfed into the stronger vortices and becomes biassed. The stability of biassed gap flow appears to be particularly dependent on the behaviour of the separated shear layer from the slit side of the plate on the unbiassed side.

When the slit ratio is very small, where the vortex shedding from each plate is weak, the biassing of gap flows at a high Reynolds number seems to be caused by a Coanda effect between the jet-like gap flow and the outside flow around the flat-plate row.

The authors wish to express sincere gratitude to Mr Kiichiro Sada and Mr Katsuhiko Yoshida for the technical assistance in making the experiment. This work was partly supported by a grant from the Ministry of Education, Science and Culture of Japan.

REFERENCES

BEARMAN, P. W. 1967 The effect of base bleed on the flow behind a two-dimensional model with a blunt trailing edge. *Aero Q.* **18**, 207–224.

BEARMAN, P. W. & TRUEMAN, D. M. 1972 An investigation of the flow around rectangular cylinders. *Aero Q.* **23**, 229–237.

BEARMAN, P. W. & WADCOCK, A. J. 1973 The interaction between a pair of circular cylinders normal to a stream. *J. Fluid Mech.* **61**. 499–511.

BIERMANN, D. & HERRNSTEIN, W. H. 1933 The interference between struts in various combinations. *NASA TR* 468, pp. 515–524.

CASTRO, I. P. 1971 Wake characteristics of two-dimensional perforated plates normal to an air-stream. *J. Fluid Mech.* **46**, 599–609.

HAYASHI, M. 1972 On the wake vortices behind rectangular cylinders at low Reynolds numbers. *Tech. Rep. Kyushu Univ.* 45, no. 6, pp. 936–942 (in Japanese).

HAYASHI, M., SAKURAI, A. & OHYA, Y. 1983 Numerical and experimental studies of wake interference of two normal flat plates at low Reynolds numbers. *Memoirs of the Faculty of Enginering, Kyushu Univ.* **43**, 165–177.

HONJI, H. 1973*a* Viscous flows past a group of circular cylinders. *J. Phys. Soc. Japan* **34**, 821–828.

HONJI, H. 1973*b* Formation of a reversed flow bubble in the time-mean wake of a row of circular cylinders. *J. Phys. Soc. Japan* **35**, 1533–1536.

HORI, E. 1959 Experiments of flow around a pair of parallel circular cylinders. In *Proc. 9th Japan Nat. Cong. Appl. Mech.*, pp. 231–234.

ISHIGAI, S., NISHIKAWA, E., NISHIMURA, K. & CHO, K. 1972 Experimental study on structure of gas flow in tube banks with tube axes normal to flow. Part 1. Kármán vortex flow around two tubes at various spacings. *Bull. JSME* **15**, 949–956.

KAMEMOTO, K. 1976 Formation and interaction of two parallel vortex streets. *Bull. JSME* **19**, 283–290.

KAMEMOTO, K. & BEARMAN, P. W. 1980 An inviscid model of interactive vortex-shedding behind a pair of flat plates arranged side by side to approaching flow. *Trans. JSME* **46**, 1229–1236.

MIZOTA, T. 1978 A technique for measuring unsteady flow velocities in the separated region. *Trans. JSCE* **10**, 77–80.

NAKAGUCHI, H., HASHIMOTO, K. & MUTO, S. 1968 An experimental study on aerodynamic drag of rectangular cylinders. *J. Japan Soc. Aero. & Space Sci.* **16**, 1–5 (in Japanese).

OHYA, Y. 1983 Wake interference of a row of normal flat plates arranged side by side in a uniform flow. Ph.D. thesis, Kyushu University (in Japanese).

OKAJIMA, A. & SUGITANI, K. 1980 Fluid characteristics of a pair of circular cylinders normal to a uniform flow at very high Reynolds numbers. *Bull. Res. Inst. Appl. Mech., Kyushu Univ.* **53**, 37–64 (in Japanese).

QUADFLIEG, H. 1977 Wirbelinduzierte Belastungen eines Zylinderpaares in inkompressibler Strömung bei großen Reynoldszahlen. *Forsch. Ing.-Wes.* **43**, 9–18.

SPIVACK, H. M. 1946 Vortex frequency and flow pattern in the wake of two parallel cylinders at varied spacing normal to an air stream. *J. Aero. Sci.* **13**, 289–301.

STANSBY, P. K. 1981 A numerical study of vortex shedding from one and two circular cylinders. *Aero Q.* **32**, 48–71.

TRITTON, D. J. 1977 *Physical Fluid Dynamics.* Van Nostrand Reinhold.

WOOD, C. J. 1964 The effect of base bleed on a periodic wake. *J. R. Aero. Soc.* **68**, 477–482.

ZDRAVKOVICH, M. M. 1977 Review of flow interaction between two circular cylinders in various arrangements. *Trans. ASME* I: *J. Fluids Engng* **99**, 618–632.